crystals

MDPI

Article

Electrochemical Performance of 2D-Hierarchical Sheet-Like $ZnCo_2O_4$ Microstructures for Supercapacitor Applications

Kumcham Prasad [1], Gutturu Rajasekhara Reddy [1], Megala Rajesh [2], P. Reddi Babu [2], Gnanendra Shanmugam [3,*], N. John Sushma [4], M. Siva Pratap Reddy [5,*], Borelli Deva Prasad Raju [2,*] and Koduru Mallikarjuna [6,7]

1 Department of Instrumentation, Sri Venkateswara University, Tirupati 517502, India; kumchamprasad91@gmail.com (K.P.); guttururajasekharareddy@gmail.com (G.R.R.)
2 Department of Physics, Sri Venkateswara University, Tirupati 517502, India; megalarajesh999@gmail.com (M.R.); reddimsc444@gmail.com (P.R.B.)
3 Department of Biotechnology, Yeungnam University, Gyeongsan, Gyeongbuk 38541, Korea
4 Department of Biotechnology, Sri Padmavati Mahila Visvavidyalayam (Women's University), Tirupati 517502, India; johnsushma@gmail.com
5 School of Electronics Engineering, Kyungpook National University, Daegu 41566, Korea
6 Department for Management of Science and Technology Development, Ton Duc Thang University, Ho Chi Minh City 758307, Vietnam; koduru.mallikarjuna@tdtu.edu.vn
7 Faculty of Applied Sciences, Ton Duc Thang University, Ho Chi Minh City 758307, Vietnam
* Correspondence: gnani@ynu.ac.kr (G.S.); drmspreddy@knu.ac.kr (M.S.P.R.); drdevaprasadraju@gmail.com (B.D.P.R.)

Received: 20 May 2020; Accepted: 26 June 2020; Published: 1 July 2020

Abstract: With the rapid improvement of the global economy, the role of energy has become even more vital in the 21st century. In this regard, energy storage/conversion devices have become a major, worldwide research focus. In response to this, we have prepared two-dimensional (2D)-hierarchical sheet-like $ZnCo_2O_4$ microstructures for supercapacitor applications using a simple hydrothermal method. The 2D-hierarchical sheet-like morphologies with large surface area and smaller thickness enhanced the contact area of active material with the electrolyte, which increased the utilization rate. We investigated the electrochemical performance of sheet-like $ZnCo_2O_4$ microstructures while using Cyclic voltammetry (CV), Galvanostatic charge-discharge (GCD), and Electrochemical impedance spectroscopy (EIS) analysis. The electrochemical results demonstrated that the $ZnCo_2O_4$ electrode possesses 16.13 mF cm^{-2} of areal capacitance at 10 μA cm^{-2} of current density and outstanding cycling performance (170% of capacitance is retained after 1000 cycles at 500 μA cm^{-2}). The high areal capacitance and outstanding cycling performance due to the unique sheet-like morphology of the $ZnCo_2O_4$ electrode makes it an excellent candidate for supercapacitor applications.

Keywords: supercapacitors; hydrothermal method; areal capacitance; sheet-like $ZnCo_2O_4$

1. Introduction

It is necessary to generate energy from renewable and inexhaustible energy sources in response to the rapid growth of global energy consumption and increasing climate changes, such as global warming and air pollution caused by non-renewable energy consumption. The energy that is produced from the renewable sources, like wind, solar, and tidal, etc., has become important due to the aforementioned global issues and rapidly increasing energy needs of the modern human society. However, this energy is still minimal and intermittent. Under these circumstances, it is necessary to well develop the clean

and highly efficient energy storage technology to enable continuous and more stable supply of energy from renewable energy sources. Among all of the clean energy technologies, Supercapacitors (SCs) are considered as one of the best candidates for energy storage/conversion systems in the near future because of their high-power density, long cycle stability, fast charging capability, small size, safe operation, low maintenance, and eco-friendly characteristics. However, the successful exploitation of renewable energy sources needs more efficient, reliable, low cost, and eco-friendly energy storage devices. SCs have been used in various applications, such as hybrid electric vehicles, industrial power grids, military equipment, etc. However, the low energy density of SCs prevents their use in many applications. Most of the current research work is focused on increasing the energy density of SCs to overcome this limitation and make them comparable to batteries [1–4].

Electric double-layer capacitors (EDLCs) and pseudocapacitors (PCs) are the two main classifications of supercapacitors and they are distinguished by their energy storage mechanisms. For EDLCs, the charge is stored at the electrode/electrolyte interface due to reversible electrolyte ion adsorption (non-Faradaic), but, for PCs, the charge is stored due to rapid, reversible Faradaic redox reactions of the active material [5]. Carbonaceous materials, such as carbon nanotubes (CNTs), mesoporous carbon, activated carbon, and graphene nanosheets are used for EDLCs, due to their higher surface area, low cost, and greater number of established fabrication techniques when compared to other materials, whereas several metal oxides/hydroxides with various nanostructured morphologies have been investigated for PCs. There has been extensive research, which has focused on pseudocapacitive materials as compared to carbon-based EDLC materials due to their high energy density [6,7]. Electrode materials are one of the important factors for improving the electrochemical performance of supercapacitors. Generally, electrode materials are classified into carbonaceous materials, conductive polymers, and transition metal oxides. The application of supercapacitors as electrode material has decreased due to the low specific capacity of carbonaceous materials and mechanical deterioration of conductive polymers. Transition metal oxides have been widely studied as electrode materials due to their high theoretical specific capacitance and abundant oxidation states. Binary transition metal oxides with their rich redox chemistry and ability to use the advantages of both metal ions, provide higher specific capacities, especially when compared to single-component metal oxides [8]. In this scenario, the electrochemical properties of two-dimensional nanostructured materials with large specific surface areas, higher surface-to-volume ratios, and shorter ion transportation channels, which provide more surface area for accessibility of the electrolyte and are more suitable than traditional bulk materials for supercapacitor applications [9–11]. Binary transitional metal oxides, such as $ZnCo_2O_4$ [12], $NiCo_2O_4$ [13], $CuCo_2O_4$ [14], $ZnFe_2O_4$ [15], and $MnCo_2O_4$ [16], have been broadly explored for their application as advanced supercapacitor electrode materials owing to their excellent properties regarding electrochemical analysis. In particular, cubic spinel-structured $ZnCo_2O_4$ has received much attention, due to its environmentally benign nature, low cost, easy preparation, controllable morphology, and good electrochemical properties [17,18].

Presently, there have been many reports on $ZnCo_2O_4$- based supercapacitors with theoretical and practical evidence. They include $ZnCo_2O_4$ micro-flowers and micro-sheets [8], $ZnCo_2O_4$ nanorods [9], $ZnCo_2O_4$ nanoflakes [19], $ZnCo_2O_4$ porous microspheres [20]. $ZnCo_2O_4$ nanosheets [21], $ZnCo_2O_4$ nanowires [22], and $ZnCo_2O_4$ nanotubes [23]. Among the various morphologies of $ZnCo_2O_4$, the sheet-like morphologies with high specific surface area and smaller thickness possess high electronic conductivity [24]. However, improving the cycling stability and energy density is necessary in the electrode material for supercapacitors [25]. In this view, we have chosen to prepare 2D-hierarchical sheet-like $ZnCo_2O_4$ microstructures while using hexamethylenetetramine (HMTA) as a surfactant via a simple hydrothermal synthesis method. Based on various analysis techniques, the as prepared material shown good pseudocapacitor properties for supercapacitor applications.

2. Materials and Methods

2.1. Material Synthesis

Typically, 10 mmol $Zn(NO_3)_2{\cdot}6H2O$,20 mmol $Co(NO_3)_2{\cdot}6H_2O$, and 1 g of HMTA were dissolved in 35 mL of deionized water and stirred well at room temperature. Once a homogeneous clear solution formed, the solution was transferred to a 50 mL Teflon-lined stainless-steel autoclave. The autoclave was heated at 160 °C for six hours and then allowed to cool to room temperature. After the reaction was complete, the precipitate that had settled at the bottom of the autoclave was collected, washed several times with DI water, was then washed with absolute ethanol to remove residual nanoparticles debris, and then dried at 70 °C for 12 h. Finally, the nanoparticle powder was annealed at 500 °C for five hours to form sheet-like $ZnCo_2O_4$ microstructures.

HMTA is used as a structure directing agent to obtain a definite morphology. Because it is a weak base, it plays an important role in morphology direction and produce large number of hydroxyl (OH^-) ions, even at elevated temperatures. During the synthesis process, the HMTA was first dispersed homogeneously in water to produce ammonia and formaldehyde (Equation (1)). Subsequently, ammonia undergoes hydrolysis to produce a large number of hydroxyl ions (Equation (2)) [26]. At low temperatures, the Zn ions can easily coordinate with the OH^- (Equations (3) and (4)) to form $Zn(OH)_4{}^{2-}$. When the temperature gradually raised, the cobalt (Co^{2+}) and zinc (Zn^{2+}) ions react with the hydroxide ions to produce Zn-Co hydroxide particles under hydrothermal reaction conditions to form the precursors of $ZnCo_2O_4$ microstructures (Equations (5) and (6)). The final products are formed after further annealing treatment. The chemical reactions involved are as follows [27].

$$(CH_2)_6N_4 + 6H_2O \rightarrow 4NH_3 + 6HCHO \tag{1}$$

$$NH_3 + H_2O \rightarrow NH_4{}^+ + OH^- \tag{2}$$

$$Zn^{2+} + 4OH^- \rightarrow Zn(OH)_4{}^{2-} \tag{3}$$

$$Zn(OH)_4{}^{2-} \rightarrow ZnO + H_2O + 2OH^- \tag{4}$$

$$2Co^{2+} + Zn^{2+} + 6OH^- \rightarrow ZnCo_2(OH)_6 \tag{5}$$

$$ZnCo_2(OH)_6 + \frac{1}{6}\,O_2 \;\rightarrow\; ZnCo_2O_4 + 3H_2O \tag{6}$$

2.2. Materials Characterization

X-ray diffraction (XRD) analysis was carried out using a diffractometer (PANalytical X'Pert PRO, Malvern, UK) with Cu K_α (λ = 1.5405980 Å) as the radiation source at an operating voltage of 40 kV and current of 30 mA to determine the crystalline nature and phase purity of the as-prepared material over a 2θ range of 10–80°. The morphological properties were examined using a scanning electron microscope (SEM) (Model number FE-SEM, S-4800, Hitachi, Japan) and a transmission electron microscope (TEM) (Model number HRTEM, Tecnai G2 F20 S-Twin, Hillsboro, OR, USA).

The electrochemical properties of the material were studied on an electrochemical workstation (CHI 760E, CH instruments, city, state, USA) while using 1 M KOH aqueous solution as an electrolyte in a three-electrode system. A platinum wire, Ag/AgCl, and the as-prepared $ZnCo_2O_4$ were used as the counter electrode, reference electrode, and working electrode, respectively. The Ag/AgCl electrode is equipped with ceramic frit molten into the glass body with 3 M KCl solution as reservoir. The cyclic voltammetry (CV) measurements were carried out over a potential range of 0 and 0.6 V at scan rates of 5 to 100 mV s^{-1} and galvanostatic charge-discharges (GCDs) were performed at current densities from 10 to 1000 μA cm^{-2} in a potential range from 0 to 0.4 V. The electrochemical impedance spectroscopy (EIS) measurements were carried out in a frequency range from 0.001 to 100 kHz at an open circuit

potential with an AC perturbation of 5 mV amplitude. The areal capacitance (C_a) was calculated from the discharge curves according to the following equation

$$C_a = \frac{(\mathrm{I}x\Delta t)}{(\mathrm{S}x\Delta \mathrm{V})} \tag{7}$$

where I is the discharge current in Amperes, Δt is the total discharge time in secs, ΔV is the potential drop during discharge in volts, and S is the area of the glassy carbon electrode in cm^2.

2.3. GCE Preparation

To carry out the electrochemical measurements, 4 mg of active material was homogeneously suspended in 2 mL of ethanol and 10 μL of the resulting suspension was uniformly deposited on the glassy carbon electrode over an area of 0.06 cm^2. The electrochemical measurements were conducted after the electrode had been dried under an infrared lamp and then washed thoroughly with de-ionized water.

3. Results and Discussion

3.1. XRD Analysis

The crystallinity of the as-prepared $ZnCo_2O_4$ microstructures were studied by XRD analysis and they are shown in Figure 1. All of the characteristic peaks centered at 2θ values of 31.35, 36.76, 38.49, 44.67, 55.70, 59.28, and 65.23 were well indexed to the (220), (311), (222), (400), (422), (511), and (440) planes, respectively, which confirms that the prepared $ZnCo_2O_4$ microstructures are spinel and cubic phases of $ZnCo_2O_4$ with space group Fd3m (JCPDS No: 23-1390) [28]. Furthermore, some weak diffraction peaks centered at 2θ values of 31.89, 34.38, 47.49, 56.65, 62.64, and 67.38° were observed denotes the presence very less fraction of ZnO in the as-prepared sample, which was formed during the synthesis [29].

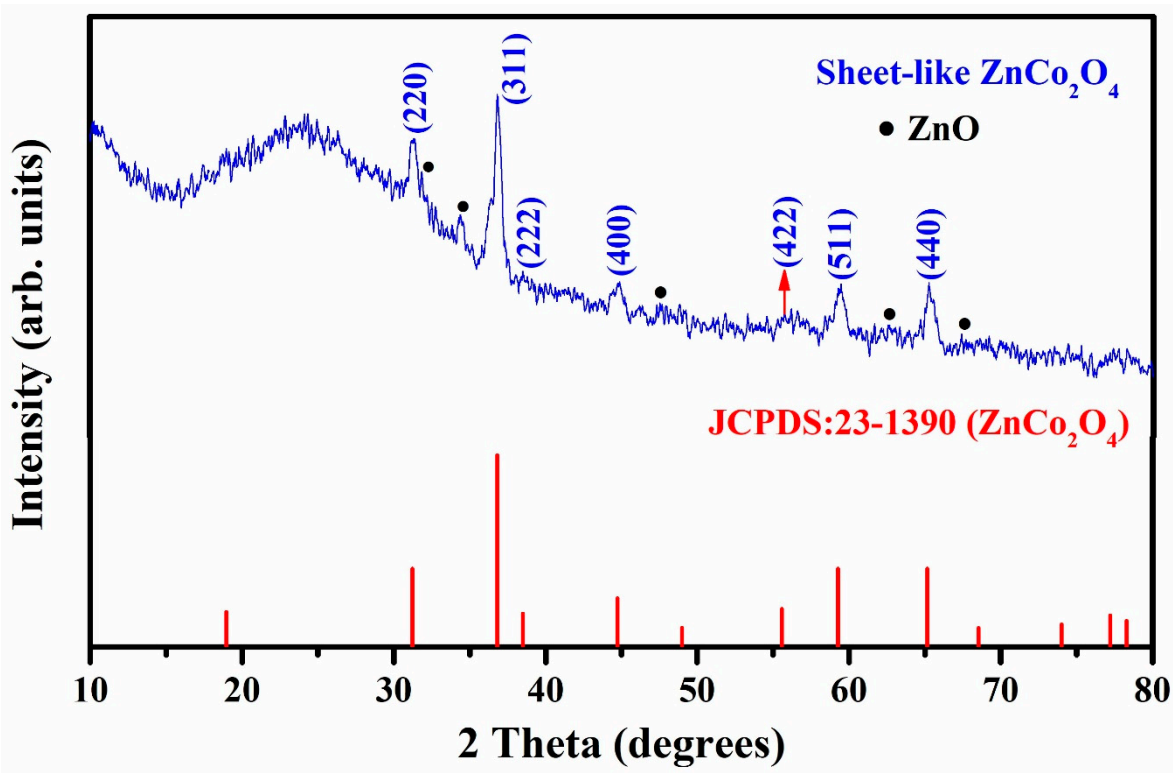

Figure 1. X-ray diffraction (XRD) pattern for sheet-like $ZnCo_2O_4$.

The XRD details of the as-prepared sheet-like $ZnCo_2O_4$ are compared with standard data and they are shown in Table 1. The average crystalline size (D) of the $ZnCo_2O_4$ sample was determined for the dominant peak (311) from XRD data using Scherrer's equation. The structural parameters such as micro strain (ε), dislocation density (δ), lattice parameter (a), cell volume (v), etc. were estimated while using the following formulae [30,31] and are shown in Table 2.

$$\text{crystalline size (D)} = \frac{K\lambda}{H cos\theta} \tag{8}$$

$$\text{micro strain } (\varepsilon) = \frac{H cos\theta}{4} \tag{9}$$

$$\text{dislocation density } (\delta) = \frac{1}{D^2} \tag{10}$$

$$2d_{hkl} \sin \theta_{hkl} = \lambda \tag{11}$$

$$\frac{1}{d^2} = \frac{h^2 + k^2 + l^2}{a^2} \tag{12}$$

$$\text{cell volume(v)} = \text{abc } \sin \beta \tag{13}$$

where K is the shape factor, D is the crystallite size in nm, θ is the peak position in degrees, H is full width at half maximum in radians, and d is the interplanar distance in Å, and h, k, and l are the Miller indices and a, b, c, and β are the lattice parameters.

Table 1. XRD data for the $ZnCo_2O_4$ microstructures.

h k l	2θ (°)		d-Spacing (Å)		JCPDS No.	Composition
	Standard Value	Observed Value	Standard Value	Observed Value		
220	31.21	31.28	2.86	2.85	23–1390	$ZnCo_2O_4$
311	36.80	36.85	2.44	2.41		
222	38.48	38.51	2.42	2.33		
422	55.57	55.74	1.62	1.64		
511	59.28	59.34	1.55	1.56		
440	65.14	65.32	1.42	1.43		

Table 2. Structural parameters of the $ZnCo_2O_4$ microstructures.

Physical Quantity (Symbol) (Units)	Value
Lattice parameter (a) (Å)	8.35
Micro strain (ε) × 10^{-3}	1.53
Dislocation density (δ) × 10^{-15}	1.96
Cell volume (v) (≈nm^3)	0.5823
Crystalline size (D) (nm)	22.6

The poor crystallinity and small crystallite size of the material, as evidenced by the sharp and broadened diffraction peaks, play an important role in enhancing the electrochemical behavior of the electrode material. This can be attributed to the availability of more transportation channels in a poor crystalline material than in a highly crystalline one, which is an essential factor for supercapacitor electrode material [32,33].

3.2. Morphological Analysis

The morphological characteristics of the $ZnCo_2O_4$ sample were investigated via SEM and TEM analyses. From the SEM images (Figure 2a,b), it is clear that the $ZnCo_2O_4$ microstructures are composed of two-dimensional (2D) hierarchical sheet-like morphologies with unequal sizes and these sheets are composed of numerous irregular pores that were generated during the annealing treatment of the sample at 500 °C in air. The high aspect ratios and surface-to-volume ratios of the loosely stacked unique 2D hierarchical sheet-like structures result in the availability of more surface area for the electrolyte and lead to enhanced utilization rates, which increase the supercapacitor performance of the electrode material [34].

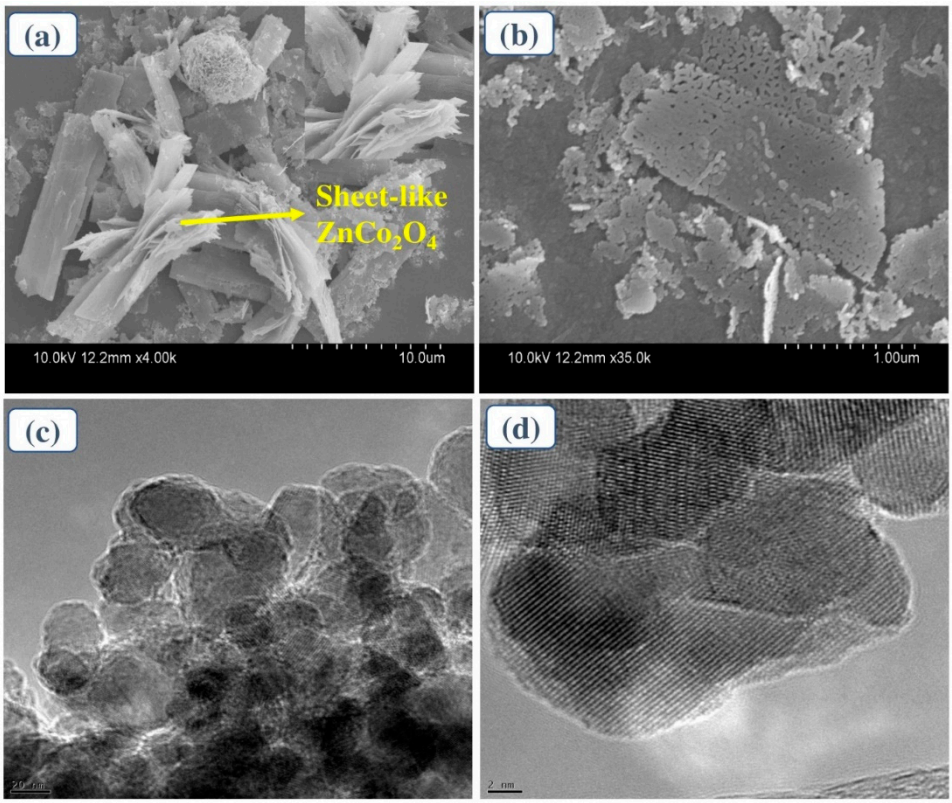

Figure 2. Scanning electron microscope (SEM) (**a**,**b**) and HR-TEM (**c**,**d**) images of sheet-like $ZnCo_2O_4$ (inset clearly shows the sheet-like structures).

Generally, the significant parameters such as shape, size, and structure play an effective role in applications, such as catalysis, energy storage/conversion, and sensor applications. In particular, the 2D-structure with a porous nature strongly influences the interaction with surrounding molecules. Surface chemistry can definitely modify the interactions between neighboring molecules, which significantly enhances the energy storage capacity in supercapacitor applications. Furthermore, this porous nature can also influence free accessing liquid electrolytes with low-dimension surface atoms. Additionally, the small atoms and high surface curvature (sharp edges) are beneficial for more reactions with nearby atoms.

A detailed evaluation of particle morphology was analyzed through HR-TEM analysis. Figure 2c,d shows the high- and low-magnification HR-TEM images. It can be observed that, based on the self-assembly process, the nanoparticles agglomerate to form sheet-like microstructures and their porous nature can also be confirmed, which is consistent with the SEM analysis. The porous nature of the material helps to provide a greater specific surface area and shortens the ion diffusion lengths between the electrode and electrolyte. This increases the number of active redox sites and their

utilization rate, which leads to the enhanced supercapacitor performance of the sheet-like $ZnCo_2O_4$ microstructure electrode [35].

3.3. Electrochemical Analysis

CV, GCD, and EIS were used to assess the supercapacitance characteristics of the sheet-like $ZnCo_2O_4$ electrode in 1M KOH while using a three-electrode electrochemical cell. Figure 3a shows the CV curves of the sheet-like $ZnCo_2O_4$ electrode at different scan rates, which ranged from 5 to 100 mV s^{-1} within a potential window of 0 to 0.6 V.

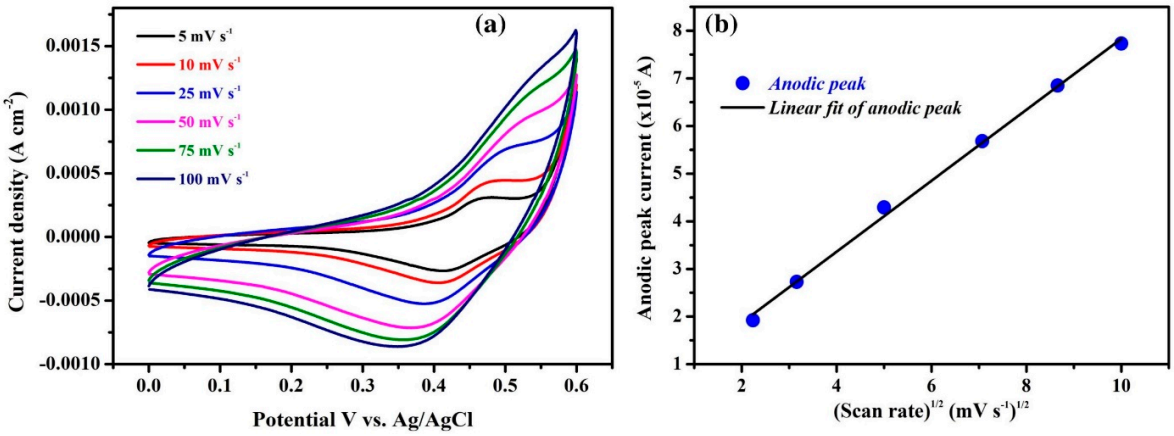

Figure 3. Cyclic voltammetry (CV) curves at different scan rates (**a**) and anodic peak current vs. the square root of the corresponding scan rate (**b**) for sheet-like $ZnCo_2O_4$.

Clearly, the pseudocapacitive behavior of the electrode can be confirmed by the pair of redox peaks that can be observed in all of the CV curves that cannot be observed in electrical double-layer capacitance. A pair of oxidation and reduction peaks are observed at 0.47 V and 0.42 V, respectively, at a scan rate of 5 mVs^{-1}. As the scan rate increased from 5 to 100 mV s^{-1}, the oxidation and reduction peaks shifted towards higher and lower potentials, respectively, indicating that the reaction kinetics are reversible due to the polarization and ohmic resistance of the material during the redox process. The faradaic redox reactions of the material is related to Co–O/Co–O–OH [36]. The possible redox reactions in the KOH electrolyte are mainly associated with the following equations:

$$Co(OH)_2 + OH^- \rightarrow CoOOH + H_2O + e^- \quad (14)$$

$$CoOOH + OH^- \rightarrow CoO_2 + H_2O + e^- \quad (15)$$

Figure 3b shows the variations of the anodic peak current as a function of the scan rate. The anodic peak current increases linearly with increasing scan rate and the area of the CV curves also increases with increasing scan rates, which demonstrates that the redox reaction is a diffusion-controlled process that is an important factor for the pseudocapacitive nature of supercapacitors [37].

Figure 4 shows the GCD curves for the as-prepared electrode at current densities that range from 10 to 1000 μA cm^{-2} within a potential window of 0–0.4 V. The non-linear charge/discharge curves obtained from GCD represent typical pseudocapacitive behavior due to the faradaic redox reactions occur at the electrode/electrolyte interface and are in good agreement with the CV analysis [38].

The areal capacitance values of the sheet-like $ZnCo_2O_4$ microstructure electrode were estimated using Formula 7 and are shown in Table 3. Figure 4b shows the variations in calculated areal capacitance values as a function of various current densities.

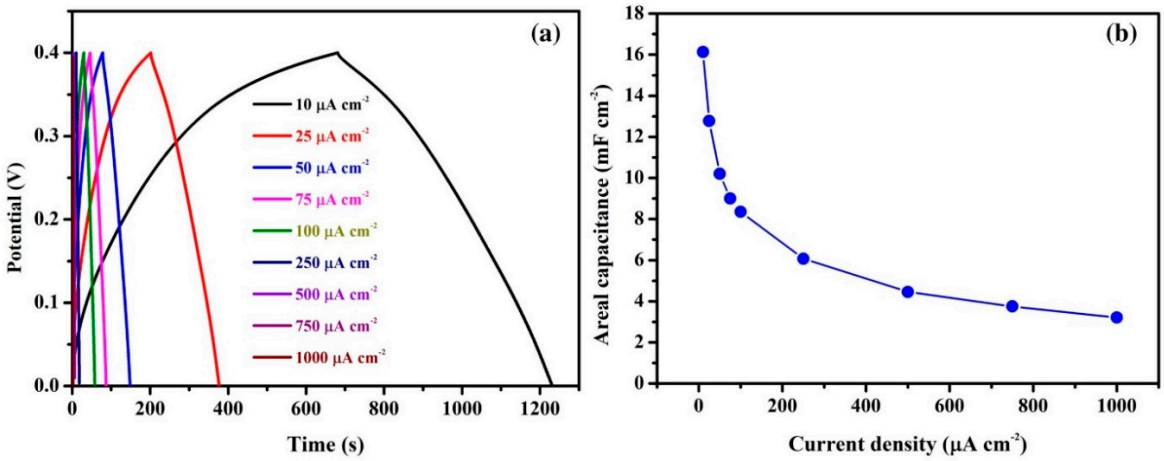

Figure 4. Galvanostatic charge-discharge (GCD) curves at various current densities (**a**) and calculated areal capacitance values with respect to various current densities (**b**) for sheet-like $ZnCo_2O_4$.

Table 3. Areal capacitance values of the sheet-like $ZnCo_2O_4$ microstructure electrode.

Current Density (μAcm^{-2})	10	25	50	75	100	250	500	750	1000
Areal Capacitance (mFcm^{-2})	16.13	12.78	10.20	9.09	8.35	6.07	4.46	3.73	3.21

The decrease in areal capacitance with current density might be due to the internal resistance and polarization of the electrode as well as the mechanical stress that is caused by insertion and removal of electrolyte ions [39].

The supercapacitor performance of the $ZnCo_2O_4$ electrode was further investigated by cyclic stability. Figure 5 shows the cyclic stability of a sheet-like $ZnCo_2O_4$ electrode at a constant current density of 500 μA cm^{-2} for 1000 charge-discharge cycles within a potential window of 0 to 0.4 V.

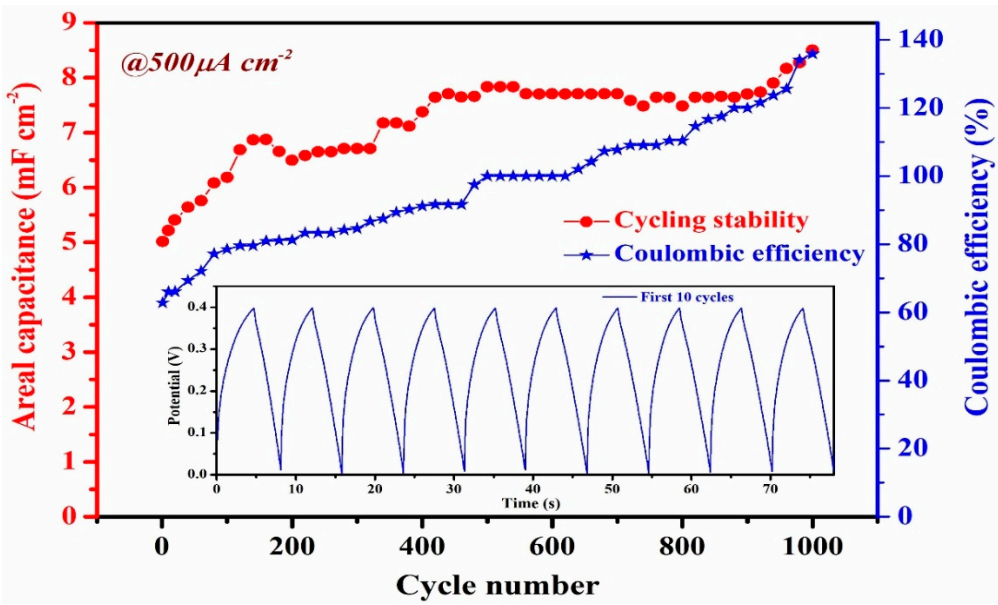

Figure 5. Cycling performance and Coulombic efficiency of sheet-like $ZnCo_2O_4$ (inset shows GCD curves for the first ten cycles).

Remarkably, approximately 170% of the areal capacitance was retained after 1000 cycles and it signifies the outstanding cycling stability of the as-prepared electrode. The increase in areal capacitance after cycling might be due to the full activation of the $ZnCo_2O_4$ electrode material. This is a phenomenon

commonly observed in transition metal oxides. The activation process of the electrode is due to the slow insertion of the electrolyte into the bulk structure of the material and the diffusion of ions by some circulation to form a greater number of active sites within the electrode material [40]. The coulombic efficiency (η) for the sheet-like $ZnCo_2O_4$ microstructures is calculated while using the following equation [41].

$$\eta = \frac{t_d}{t_c} \times 100\% \tag{16}$$

where t_d and t_c are the discharge and charge times in secs, respectively.

Figure 5 also shows the coulombic efficiency of the electrode for 1000 cycles, which was retained at approximately 135% and indicates the suitability of the material for supercapacitors with long-term cycling stability [42]. The symmetry of the shapes of the GCD curves for the first 10 cycles (inset of Figure 5) indicates good reversible redox behavior of the electrode [43]. The areal capacitance values of different transition metal oxides with different combinations are compared with the present work and are shown in Table 4. From the comparison, our present work of sheet-$ZnCo_2O_4$ microstructures can be recommended for supercapacitor electrode application.

Table 4. Areal capacitance of different metal oxides in comparison with present work.

Different Metal Oxides and Combinations	Synthesis Method	Areal Capacitance	Reference
$NiCo_2O_4/MnO_2$	Hydrothermal	5.3 F cm^{-2} @ 1 mA cm^{-2}	[44]
$ZnCo_2O_4/Ni(OH)_2$	Electrochemical deposition	4.6 F cm^{-2} @ 2 mA cm^{-2}	[45]
$ZnCo_2O_4$	Hydrothermal	2.72 F cm^{-2} @ 2.02 mA cm^{-2}	[46]
2D-$LiCoO_2$	Electrochemical deposition	310 mF cm^{-2} @ 5 mV s^{-1}	[47]
MnO_2/MoS_2	Magnetron sputtering	224 mF cm^{-2} @ 0.1 mA cm^{-2}	[48]
$NiCo_2O_4$	Sol-gel method	40.6 mF cm^{-2} @ 0.133 mA cm^{-2}	[49]
TiO_2	Electrochemical anodization	23.24 mF cm^{-2} @ 2 mV s^{-1}	[50]
$Co(OH)_2/Ni$	Electrochemical deposition	22.9 mF cm^{-2} @ 5 mV s^{-1}	[51]
sheet-like $ZnCo_2O_4$	Hydrothermal	16.13 mF cm^{-2} @ 10 μA cm^{-2}	present

EIS was performed before and after cycling for 1000 cycles in a frequency range from 0.001 to 100 kHz in order to study the behavior of $ZnCo_2O_4$ electrode materials for supercapacitors, as shown in Figure 6. The Nyquist diagrams for both cases show a semicircle and straight line in the high and low frequency regions, respectively. These are the characteristics of ion diffusion and capacitive behavior. The diameter of the semicircle in the high-frequency region and the straight line in the low frequency region denote the charge transfer resistance that is caused by the Faradaic reactions and Warburg resistance, which are related to the electrolyte diffusion to the electrode surface.

These Nyquist plots are fitted to the equivalent circuit (Inset of Figure 6). The R_s, R_{ct} values are measured from the fitting and are shown in Table 5. The decrease in R_s, R_{ct} represents that the $ZnCo_2O_4$ electrode material has excellent ionic conductivity and faster charge-transfer rates after 1000 cycles, indicates the enhanced electrochemical performance of the material [52,53].

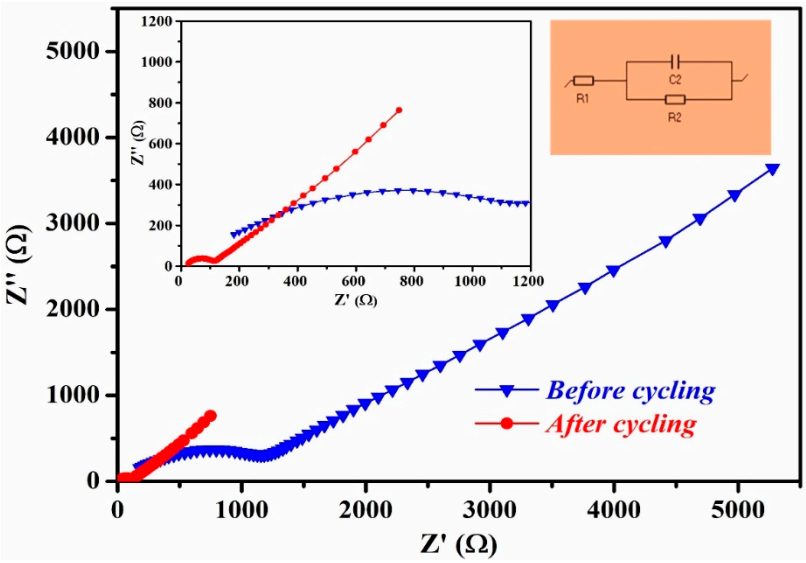

Figure 6. Niquist plots for sheet-like $ZnCo_2O_4$ before and after 1000 cycles. Inset shows the magnified images for sheet-like $ZnCo_2O_4$ and fit circuit diagram (R_1—the series resistance (R_s), R_2—the charge transfer resistance (R_{ct}) and C_2—the constant phase element of the circuit.).

Table 5. Series resistance (R_s) and charge transfer resistance (R_{ct}) of sheet-like $ZnCo_2O_4$ before and after cycling.

Resistance	Before Cycling	After Cycling
(Ω)	242.2	30.11
(Ω)	1160	110

4. Conclusions

In summary, 2D-hierarchical sheet-like $ZnCo_2O_4$ microstructures were prepared via a simple hydrothermal synthesis method while using HMTA as a surfactant. The as prepared material was systematically studied via various analytical techniques. The XRD analysis confirmed the crystalline nature of the sample. The SEM images indicated a 2D sheet-like morphology, which was confirmed by the HR-TEM analysis. The as-prepared $ZnCo_2O_4$ electrode delivered good electrochemical properties in a 1 M KOH electrolyte solution. An areal capacitance of 16.13 mF cm^{-2} was delivered at a current density of 10 μA cm^{-2}. The electrode also achieved an outstanding cycling performance of 170% capacitance retention and coulombic efficiency of 135% after 1000 cycles at 500 μA cm^{-2}. The unique 2D hierarchical sheet-like structure with a porous material nature helped to achieve the above-mentioned properties. Finally, the facile synthesis method, along with the unique structural properties and good electrochemical characteristics of the sheet-like $ZnCo_2O_4$ microstructures, can be considered as a favorable electrode material for supercapacitor applications.

Author Contributions: K.P. Formal analysis, Data curation, Investigation, Methodology, Writing-original draft, G.R.R. Investigation, Writing-review & editing, M.R. Data curation, Methodology, P.R.B. Methodology, G.S. Resources, Writing-review & editing, N.J.S. Data curation, Funding acquisition, Writing-original draft, Writing-review & editing, M.S.P.R. Data curation, Funding acquisition, Resources, Writing-review & editing, B.D.P.R. Conceptualization, Data curation, Funding acquisition, Supervision, Resources, Writing-original draft, Writing-review & editing, K.M. Writing-review & editing. All authors have read and agreed to the published version of the manuscript.

Funding: This work was supported by the National Research Foundation of Korea funded by the Ministry of Science, ICT and Fusion Research (NRF-2018R1D1A1B07040603) and BK21 Plus funded by the Ministry of Education (21A20131600011).

Acknowledgments: The author Kumcham Prasad is highly grateful to UGC, Govt. of India for providing financial assistance in the form of Rajiv Gandhi National Fellowship for pursuing Ph. D program.

Conflicts of Interest: The authors declare no conflict of interest.

References

1. Guo, D.; Zhang, H.; Yu, X.; Zhang, M.; Zhang, P.; Li, Q.; Wang, T. Facile synthesis and excellent electrochemical properties of $CoMoO_4$ nanoplate arrays as supercapacitors. *J. Mater. Chem. A* **2013**, *1*, 7247–7254. [CrossRef]
2. Hou, L.; Hua, H.; Liu, S.; Pang, G.; Yuan, C. Surfactant-assisted hydrothermal synthesis of ultrafine $CoMoO_4{\cdot}0.9H_2O$ nanorods towards high-performance supercapacitors. *New J. Chem.* **2015**, *39*, 5507–5512. [CrossRef]
3. Kazemi, S.H.; Tabibpour, M.; Kiani, M.A.; Kazemi, H. An advanced asymmetric supercapacitor based on a binder-free electrode fabricated from ultrathin $CoMoO_4$ nano-dandelions. *RSC Adv.* **2016**, *6*, 71156–71164. [CrossRef]
4. Xu, K.; Chao, J.; Li, W.; Liu, Q.; Wang, Z.; Liu, X.; Zou, R.; Hu, J. $CoMoO_4{\cdot}0.9H_2O$ nanorods grown on reduced graphene oxide as advanced electrochemical pseudocapacitor materials. *RSC Adv.* **2014**, *4*, 34307–34314. [CrossRef]
5. Candler, J.; Elmore, T.; Gupta, B.K.; Dong, L.; Palchoudhury, S.; Gupta, R.K. New insight into higherature driven morphology reliant $CoMoO_4$ flexible supercapacitors. *New J. Chem.* **2015**, *39*, 6108–6116. [CrossRef]
6. Mandal, M.; Ghosh, D.; Giri, S.; Shakir, I.; Das, C.K. Polyaniline-wrapped 1D $CoMoO_4{\cdot}0.75H_2O$ nanorods as electrode materials for supercapacitor energy storage applications. *RSC Adv.* **2014**, *4*, 30832–30839. [CrossRef]
7. Veerasubramani, G.K.; Krishnamoorthy, K.; Radhakrishnan, S.; Kim, N.J.; Kim, S.J. Synthesis, characterization, and electrochemical properties of $CoMoO_4$ nanostructures. *Int. J. Hydrogen Energy* **2014**, *39*, 5186–5193. [CrossRef]
8. Pan, Y.; Gao, H.; Zhang, M.; Li, L.; Wang, Z. Facile synthesis of $ZnCo_2O_4$micro-flowers and micro-sheets on Ni foam for pseudocapacitor electrodes. *J. Alloys Compd.* **2017**, *702*, 381–387. [CrossRef]
9. Wu, X.; Meng, L.; Wang, Q.; Zhang, W.; Wang, Y. Highly flexible and large areal/volumetric capacitances for asymmetric supercapacitor based on $ZnCo_2O_4$ nanorods arrays and polypyrrole on carbon cloth as binder-free electrodes. *Mater. Lett.* **2019**, *234*, 1–4. [CrossRef]
10. Ray, A.; Roy, A.; Saha, S.; Das, S. Transition Metal Oxide-Based Nano-materials for Energy Storage Application. *Sci. Technol. Adv. Appl. Supercapacitors* **2019**, 1–17, IntechOpen. [CrossRef]
11. Zhang, Q.; Uchaker, E.; Candelaria, S.L.; Cao, G. Nanomaterials for energy conversion and storage. *Chem. Soc. Rev.* **2013**, *42*, 3127–3171. [CrossRef] [PubMed]
12. Guan, B.; Guo, D.; Hu, L.; Zhang, G.; Fu, T.; Ren, W.; Li, J.; Li, Q. Facile synthesis of $ZnCo_2O_4$nanowire cluster arrays on Ni foam for high-performance asymmetric supercapacitors. *J. Mater. Chem. A* **2014**, *2*, 16116–16123. [CrossRef]
13. Cheng, M.; Fan, H.; Song, Y.; Cui, Y.; Wang, R. Interconnected hierarchical $NiCo_2O_4$ microspheres as high-performance electrode materials for supercapacitors. *Dalt. Trans.* **2017**, *46*, 9201–9209. [CrossRef] [PubMed]
14. Ensafi, A.A.; Moosavifard, S.E.; Rezaei, B.; Kaverlavani, S.K. Engineering onion-like nanoporous $CuCo_2O_4$ hollow spheres derived from bimetal-organic frameworks for high-performance asymmetric supercapacitors. *J. Mater. Chem. A* **2018**, *6*, 10497–10506. [CrossRef]
15. Raut, S.S.; Sankapal, B.R. First report on synthesis of $ZnFe_2O_4$ thin film using successive ionic layer adsorption and reaction: Approach towards solid-state symmetric supercapacitor device. *Electrochim. Acta* **2016**, *198*, 203–211. [CrossRef]
16. Ji, Y.; Xie, J.; Wu, J.; Yang, Y.; Fu, X.Z.; Sun, R.; Wong, C.P. Hierarchical nanothorns $MnCo_2O_4$ grown on porous/dense Ni bi-layers coated Cu wire current collectors for high performance flexible solid-state fiber supercapacitors. *J. Power Sources* **2018**, *393*, 54–61. [CrossRef]
17. Jinlong, L.; Tongxiang, L. The effects of urea concentration on microstructures of $ZnCo_2O_4$ and its supercapacitor performance. *Ceram. Int.* **2017**, *43*, 6168–6174. [CrossRef]
18. Zhao, J.; Li, C.; Zhang, Q.; Zhang, J.; Wang, X.; Lin, Z.; Wang, J.; Lv, W.; Lu, C.; Wong, C.; et al. An all-solid-state, lightweight, and flexible asymmetric supercapacitor based on cabbage-like $ZnCo_2O_4$ and porous VN nanowires electrode materials. *J. Mater. Chem. A* **2017**, *5*, 6928–6936. [CrossRef]

19. Cheng, J.; Lu, Y.; Qiu, K.; Yan, H.; Hou, X.; Xu, J.; Han, L.; Liu, X.; Kim, J.K.; Luo, Y. Mesoporous $ZnCo_2O_4$ nanoflakes grown on nickel foam as electrodes for high performance supercapacitors. *Phys. Chem. Chem. Phys.* **2015**, *17*, 17016–17022. [CrossRef]
20. Gai, Y.; Shang, Y.; Gong, L.; Su, L.; Hao, L.; Dong, F. A self-template synthesis of porous $ZnCo_2O_4$ microspheres for high-performance quasi-solid-state asymmetric supercapacitors. *RSC Adv.* **2016**, *7*, 1038–1044. [CrossRef]
21. Bao, F.; Wang, X.; Zhao, X.; Wang, Y.; Ji, Y.; Zhang, H.; Liu, X. Controlled growth of mesoporous $ZnCo_2O_4$ nanosheet arrays on Ni foam as high-rate electrodes for supercapacitors. *RSC Adv.* **2014**, *4*, 2393–2397. [CrossRef]
22. Wang, S.; Pu, J.; Tong, Y.; Cheng, Y.; Gao, Y.; Wang, Z. $ZnCo_2O_4$ nanowire arrays grown on nickel foam for high-performance pseudocapacitors. *J. Mater. Chem. A* **2014**, *2*, 5434–5440. [CrossRef]
23. Luo, W.; Hu, X.; Sun, Y.; Huang, Y. Electrospun porous $ZnCo_2O_4$ nanotubes as a high-performance anode material for lithium-ion batteries. *J. Mater. Chem.* **2012**, *22*, 8916–8921. [CrossRef]
24. Zhou, Y.; Chen, L.; Jiao, Y.T.; Li, Z.; Gao, Y. Controllable fabrication of $ZnCo_2O_4$ ultra-thin curved sheets on Ni foam for high-performance asymmetric supercapacitors. *Electrochim. Acta* **2019**, *299*, 388–394. [CrossRef]
25. Simon, P.; Gogotsi, Y.; Simon, P. 08nature mater-Materials for electrochemical capacitors.PDF. *Nat. Mater.* **2008**, *7*, 845–854. [CrossRef] [PubMed]
26. Hussain, S.K.; Yu, J.S. HMTA-assisted uniform cobalt ions activated copper oxide microspheres with enhanced electrochemical performance for pseudocapacitors. *Electrochim. Acta* **2017**, *258*, 388–395. [CrossRef]
27. Xu, L.; Zhao, Y.; Lian, J.; Xu, Y.; Bao, J.; Qiu, J.; Xu, L.; Xu, H.; Hua, M.; Li, H. Morphology controlled preparation of $ZnCo_2O_4$ nanostructures for asymmetric supercapacitor with ultrahigh energy density. *Energy* **2017**, *123*, 296–304. [CrossRef]
28. Li, X.; Zhang, M.; Wu, L.; Fu, Q.; Gao, H. Annealing temperature dependent $ZnCo_2O_4$ nanosheet arrays supported on Ni foam for high-performance asymmetric supercapacitor. *J. Alloys Compd.* **2019**, *773*, 367–375. [CrossRef]
29. Lahure, P.; Salunke, P.; Soliwal, R.; Yadav, A.; Tripathi, S.; Koser, A.A. X-Ray Diffraction Study of ZnO Nanoparticles. *IJSRPAS* **2015**, *3*, 32–33.
30. Priya, M.; Premkumar, V.K.; Vasantharani, P.; Sivakumar, G. Structural and electrochemical properties of $ZnCo_2O_4$ nanoparticles synthesized by hydrothermal method. *Vacuum* **2019**, *167*, 307–312. [CrossRef]
31. Hossen, M.M.; Hossen, M.B. Structural, electrical and magnetic properties of $Ni_{0.5}Cu_{0.2}Cd_{0.3}La_xFe_{2\text{-}x}O_4$ nano-ferrites due to lanthanum doping in the place of trivalent iron. *Phys. B Condens. Matter* **2020**, *585*, 412116. [CrossRef]
32. Kianpour, G.; Salavati-Niasari, M.; Emadi, H. Precipitation synthesis and characterization of cobalt molybdates nanostructures. *Superlattices Microstruct.* **2013**, *58*, 120–129. [CrossRef]
33. Liu, M.C.; Kong, L.B.; Kang, L.; Li, X.; Walsh, F.C.; Xing, M.; Lu, C.; Ma, X.J.; Luo, Y.C. Synthesis and characterization of $M_3V_2O_8$ (M = Ni or Co) based nanostructures: A new family of high performance pseudocapacitive materials. *J. Mater. Chem. A* **2014**, *2*, 4919–4926. [CrossRef]
34. Chuo, H.X.; Gao, H.; Yang, Q.; Zhang, N.; Bu, W.B.; Zhang, X.T. Rationally designed hierarchical $ZnCo_2O_4/Ni(OH)_2$ nanostructures for high-performance pseudocapacitor electrodes. *J. Mater. Chem. A* **2014**, *2*, 20462–20469. [CrossRef]
35. Li, S.; Wang, Y.; Sun, J.; Zhang, Y.; Xu, C.; Chen, H. Hydrothermal synthesis of Fe-doped Co_3O_4 urchin-like microstructures with superior electrochemical performances. *J. Alloys Compd.* **2020**, *821*, 153507-1–153507-10. [CrossRef]
36. Rajesh, J.A.; Min, B.K.; Kim, J.H.; Kang, S.H.; Kim, H.; Ahn, K.S. Facile hydrothermal synthesis and electrochemical supercapacitor performance of hierarchical coral-like $ZnCo_2O_4$ nanowires. *J. Electroanal. Chem.* **2017**, *785*, 48–57. [CrossRef]
37. Tomboc, G.M.; Jadhav, H.S.; Kim, H. PVP assisted morphology-controlled synthesis of hierarchical mesoporous $ZnCo_2O_4$ nanoparticles for high-performance pseudocapacitor. *Chem. Eng. J.* **2017**, *308*, 202–213. [CrossRef]
38. Wang, X.; Li, W.; Wang, X.; Zhang, J.; Sun, L.; Gao, C.; Shang, J.; Hu, Y.; Zhu, Q. Electrochemical properties of $NiCoO_2$ synthesized by hydrothermal method. *RSC Adv.* **2017**, *7*, 50753–50759. [CrossRef]
39. Han, X.; Liao, F.; Zhang, Y.; Han, X.; Xu, C.; Chen, H. Solvothermal preparation of zinc cobaltite mesoporous microspheres for high-performance electrochemical supercapacitors. *J. Alloys Compd.* **2019**, *781*, 425–432. [CrossRef]

40. Liu, X.Y.; Zhang, Y.Q.; Xia, X.H.; Shi, S.J.; Lu, Y.; Wang, X.L.; Gu, C.D.; Tu, J.P. Self-assembled porous $NiCo_2O_4$ hetero-structure array for electrochemical capacitor. *J. Power Sources* **2013**, *239*, 157–163. [CrossRef]
41. Chang, X.; Zang, L.; Liu, S.; Wang, M.; Guo, H.; Wang, C.; Wang, Y. In situ construction of yolk-shell zinc cobaltite with uniform carbon doping for high performance asymmetric supercapacitors. *J. Mater. Chem. A* **2018**, *6*, 9109–9115. [CrossRef]
42. Shang, Y.; Xie, T.; Gai, Y.; Su, L.; Gong, L.; Lv, H. Electrochimica Acta Self-assembled hierarchical peony-like $ZnCo_2O_4$ for high-performance asymmetric supercapacitors. *Electrochim. Acta* **2017**, *253*, 281–290. [CrossRef]
43. Liu, M.C.; Kong, L.B.; Lu, C.; Li, X.M.; Luo, Y.C.; Kang, L. Facile fabrication of $CoMoO_4$ nanorods as electrode material for electrochemical capacitors. *Mater. Lett.* **2013**, *94*, 197–200. [CrossRef]
44. Su, L.; Gao, L.; Du, Q.; Hou, L.; Ma, Z.; Qin, X.; Shao, G. Construction of $NiCo_2O_4$@MnO_2 nanosheet arrays for high-performance supercapacitor: Highly cross-linked porous heterostructure and worthy electrochemical double-layer capacitance contribution. *J. Alloys Compd.* **2018**, *749*, 900–908. [CrossRef]
45. Pan, Y.; Gao, H.; Zhang, M.; Li, L.; Wang, G.; Shan, X. Three-dimensional porous $ZnCo_2O_4$ sheet array coated with $Ni(OH)_2$ for high-performance asymmetric supercapacitor. *J. Colloid Interface Sci.* **2017**, *497*, 50–56. [CrossRef] [PubMed]
46. Song, D.; Zhu, J.; Li, J.; Pu, T.; Huang, B.; Zhao, C.; Xie, L.; Chen, L. Free-standing Two-dimensional Mesoporous $ZnCo_2O_4$ Thin Sheets Consisting of 3D Ultrathin Nanoflake Array Frameworks for High Performance Asymmetric Supercapacitor. *Electrochim. Acta* **2017**, *257*, 455–464. [CrossRef]
47. Lu, J.; Ran, H.; Li, J.; Wan, J.; Wang, C.; Ji, P.; Wang, X.; Liu, G.; Hu, C. A fast composite-hydroxide-mediated approach for synthesis of 2D-$LiCoO_2$ for high performance asymmetric supercapacitor. *Electrochim. Acta* **2020**, *331*, 135426-1–135426-7. [CrossRef]
48. Zhang, H.; Wei, J.; Yan, Y.; Guo, Q.; Xie, L.; Yang, Z.; He, J.; Qi, W.; Cao, Z.; Zhao, X.; et al. Facile and scalable fabrication of MnO_2 nanocrystallines and enhanced electrochemical performance of MnO_2/MoS_2 inner heterojunction structure for supercapacitor application. *J. Power Sources* **2020**, *450*. [CrossRef]
49. Liu, Y.; Wang, N.; Yang, C.; Hu, W. Sol-gel synthesis of nanoporous $NiCo_2O_4$ thin films on ITO glass as high-performance supercapacitor electrodes. *Ceram. Int.* **2016**, *42*, 11411–11416. [CrossRef]
50. Zhang, J.; Wang, Y.; Wu, J.; Shu, X.; Yu, C.; Cui, J.; Qin, Y.; Zhang, Y.; Ajayan, P.M.; Wu, Y. Remarkable supercapacitive performance of TiO^2 nanotube arrays by introduction of oxygen vacancies. *Chem. Eng. J.* **2017**, *313*, 1071–1081. [CrossRef]
51. Soram, B.S.; Dai, J.; Kshetri, T.; Kim, N.H.; Lee, J.H. Vertically grown and intertwined $Co(OH)_2$ nanosheet@Ni-mesh network for transparent flexible supercapacitor. *Chem. Eng. J.* **2019**, *391*, 123540-1–123540-12. [CrossRef]
52. Yang, W.; Gao, Z.; Ma, J.; Wang, J.; Wang, B.; Liu, L. Effects of solvent on the morphology of nanostructured Co_3O_4 and its application for high-performance supercapacitors. *Electrochim. Acta* **2013**, *112*, 378–385. [CrossRef]
53. Jinlong, L.; Meng, Y.; Suzuki, K.; Miura, H. Synthesis of $CoMoO_4$@RGO nanocomposites as high-performance supercapacitor electrodes. *Microporous Mesoporous Mater.* **2017**, *242*, 264–270. [CrossRef]